A Two-Dimensional Wavepacket Study of the Nonadiabatic Dynamics of CH_2BrCl

Tamás Rozgonyi[†] **and Leticia González***[,‡,§]

Institute of Structural Chemistry, Chemical Research Center, Hungarian Academy of Sciences, 1025 Budapest, Pusztaszeri út 59-67, Hungary, Institut für Physikalische Chemie, Friedrich-Schiller Universität, Jena Helmholtzweg 4, 07743 Jena, Germany, and Institut für Chemie und Biochemie, Freie Universität Berlin, Takustrasse 3, 14195 Berlin, Germany

Received: February 7, 2008; Revised Manuscript Received: March 19, 2008

The nonadiabatic photodissociation dynamics of CH_2BrCl into $CH_2Br + Cl$ or $CH_2Cl + Br$ is studied using two-dimensional wavepacket propagations on ab initio multiconfigurational MS-CASPT2 potential energy surfaces. Using a three-state diabatic model, we investigate the electronic states responsible for the two competing fragmentation channels and how the conical intersection present between the two lowest excited states affects the dissociation rate. Within this model, we find that the Br/Cl branching ratio depends on the irradiation wavelength. Predominant C−Br fragmentation occurs for wavelengths longer than 200 nm, while nonadiabatic C−Cl dissociation with a constant branching ratio of 0.4 is predicted upon absorption of photons in the range of 170−180 nm. Additionally, we observe complete nonadiabatic population transfer in less than 100 fs, that is, before the wavepacket can reach the conical intersection. As a consequence, there is no three-body $CH_2 + Br + Cl$ dissociation.

1. Introduction

Halomethanes exhibit an interesting photochemistry since they deliver halogen-containing radicals to the atmosphere contributing to the stratospheric ozone destruction.[1] Upon absorption of ultraviolet (UV) light, halomethanes are excited to different electronic excited states where an electron is promoted from a lone pair of the halogen to a carbon−halogen antibonding orbital, $n(X) \rightarrow \sigma^*(C-X)$, leading to C−X dissociation. The possibility of having different channels makes dihalomethanes attractive candidates to explore the complex interplay of competing dynamical fragmentation pathways.

In particular, CH_2BrCl has been the subject of different studies because of its apparent simplicity. Nanosecond lasers combined with multiphoton ionization and time-of-flight spectroscopic techniques and velocity map imaging can be found in refs 2–4. Tzeng et al.[5] examined its photodissociation at 248 and 193 nm using photofragment translational spectroscopy. While using light of 248 nm exclusive dissociation into $CH_2Cl + Br$ products is detected, a Br/Cl branching ratio of ∼4.5 is observed with 193 nm.[5] Also, from the measured anisotropy parameter, it is concluded that the Br dissociation occurs via an $A' \rightarrow A'$ transition.

Recently, a velocity map imaging study combined with pump−probe (266/400 nm) femtosecond (fs) laser pulses has been done in the group of Janssen and Bañares.[6] The obtained ion images indicate that the fragmentation occurs on a fs time scale, yielding mainly Br radicals from neutral surfaces, while dissociative ionization is less important.[6] Zhou and co-workers have also examined the photodissociation of CH_2BrCl using time-sliced ion velocity imaging between 193.3 and 266.6 nm.[7] In their study, they propose that repulsive surfaces are responsible for the main channels $Br(^2P_{3/2})$ and $Br(^2P_{1/2})$, while the formation of $Cl(^2P_{3/2,1/2})$ ions at 235 nm comes from secondary photodissociation processes.

Ion imaging techniques applied to related halomethanes[8–11] provide strong evidence that the photodissociation dynamics of this class of molecules involves nonadiabatic transitions. A first attempt to describe the nonadiabatic photodissociation of CH_2BrCl was done by Takayanagi et al., who fitted two-dimensional (2D) model potential energy surfaces (PES) using spectroscopic data.[12] These PES, however, neither include all of the crossings between the important states nor account for conical intersections (CoIn), which, as it will be explained later, are present in the title molecule.

In our group, we have calculated for the first time the UV electronic absorption spectrum of CH_2BrCl as well as a 2D PES along the relevant C−X coordinates using high-level ab initio calculations.[13–15] In particular, we have focused on the lowest-lying singlet $\tilde{A}$ and $\tilde{B}$ bands, which we mainly associate with the b^1A' and c^1A' singlet excited states.[14] Inspection of the PES reveals an extended near-degenerate region between these two states and the presence of an accidental same symmetry CoIn.[15] This fact is in line with the assumption that nonadiabatic processes are responsible for ultrafast dissociation at particular wavelengths. Following our interest in the photodynamic behavior of this type of molecules, in this paper, we employ the PES reported in ref 15 to perform wavepacket propagations in diabatic surfaces. This should help to shed some light on the immediate dynamics following excitation at specific wavelengths. In the long-term, it appears interesting to us to design control strategies which could enhance the dissociation of the weaker bond versus the strong one, that is,which could modify the Br/Cl ratio, exploiting nonadiabatic effects. Until now, this branching ratio has been modified experimentally by Gerber and co-workers with the help of optimal feedback control.[16] A transform-limited pulse of 800 nm results in a CH_2Cl^+/CH_2Br^+ ratio of 12:1, which by optimal shaping can be modified to 6:1. As it is typical for experimental optimal feedback control, the mechanism underlying the selective dynamics is concealed.[17]

* To whom correspondence should be addressed.
[†] Chemical Research Center, Hungarian Academy of Sciences.
[‡] Friedrich-Schiller Universität.
[§] Freie Universität Berlin.

10.1021/jp8011427 CCC: $40.75
Published on Web 06/03/2008

In ref 16, it is claimed that high-lying Rydberg states could play a role for the control,[18] and taking into account the number of photons involved in that experiment, such high-lying states[14] may indeed be the key for the achieved optimal ratios.

As mentioned above, here, we shall restrict ourselves to the two lowest crossing b^1A' and c^1A' states of CH_2BrCl. With the help of wavepacket propagations, we aim at answering the following questions: i) Which states are responsible for CH_2Cl + Br and CH_2Br + Cl fragmentation channels? ii) what is the role of the conical intersection during the dissociation process? iii) how long does the nonadiabatic transition take to be completed? iv) is a three-body dissociation possible? and finally, v) how is the Br/Cl branching ratio influenced by the irradiating wavelength? These questions involve watching the evolution of the wavepacket in the b^1A' and c^1A' states. Specially the c^1A' state promises an interesting dynamics since around the region of near degeneracy, wavepacket bifurcation will occur.

The rest of the paper is organized as follows. Section II describes the theoretical background, including a brief summary of the underlying quantum chemistry, the methods used in the calculation of the vibrational eigenstates, the diabatization of the PES, and the quantum dynamical tools employed. Section III contains the numerical results, and finally, Section IV concludes this paper.

2. Theoretical Background

2.1. Ab Initio Quantum Chemistry. The electronic structure of CH_2BrCl and its ground and low-lying singlet PES have been described in detail in refs 13–15. Here, we just recall the details relevant for this work. We consider CH_2BrCl preoriented with the C atom in the origin, the Br atom placed on the z axis and the Cl in the xz plane. Assuming C_s symmetry, the electronic ground state is the a^1A' state. Higher in energy follow the a^1A'' (6.04 eV), b^1A' (6.12 eV), b^1A'' (7.11 eV), and c^1A' (7.17 eV) states.

The wave functions of the A′ and A″ states have equivalent configurations[13] and thus should exhibit a similar energetic profile and corresponding equivalent dynamical behavior. At the Franck−Condon (FC) region, the oscillator strengths of the $a^1A' \rightarrow a^1A''$ ($n_y(Br) \rightarrow \sigma^*(C-Br)$) and $a^1A' \rightarrow b^1A'$ ($n_x(Br) \rightarrow \sigma^*(C-Br)$) transitions are similar (ca. 0.008 au), and both states can, in principle, be expected to be spectroscopically populated. In contrast, the oscillator strength of the $a^1A' \rightarrow b^1A''$ transition ($n_y(Cl) \rightarrow \sigma^*(C-Cl)$) is very weak (0.005 au) compared to the value of 0.021 au of the $a^1A' \rightarrow c^1A'$ transition ($n_z(Cl) \rightarrow \sigma^*(C-Cl)$). In view that product anisotropy parameters suggest that excitations at 193 and 248 nm are dominated by $A' \rightarrow A'$ transitions[5] (vide supra) and that the dynamics of A′ and A″ states should be alike, as a first approximation, PESs have been constructed only for A′ states. Assuming that the primary dynamics takes place within hundreds of fs,[6] we also neglect neglect as a first approximation the effect of spin−orbit interactions.

With these assumptions in mind, the states of interest are a^1A', b^1A', and c^1A' . The PESs are computed at the multistate complete active space perturbation theory of second order, MS-CASPT2/CASSCF(12,12), averaged over 11 roots and with a level shift of 0.3−0.4 au. Transition dipole moment (TDM) functions are computed by the CAS state interaction method[19] from the corresponding perturbed-modified CAS (PMCAS) reference function,[20] that is, linear combinations of all CAS states involved in the MS-CASPT2 calculation. These calculations were carried out using the MOLCAS 5.0 and 6.0 quantum chemistry software.[21]

CH_2BrCl is modeled as a pseudotriatomic with two reaction coordinates, $q_1 = d(C-Br)$ and $q_2 = d(C-Cl)$. The remaining degrees of freedom are frozen to their equilibrium values and decoupled from q_1 and q_2. This decoupling is reasonable for ultrafast dissociation time scales since the energy remains in the dissociative bond and intramolecular vibrational redistribution (IVR) can be neglected (see section 3.4). The 2D PESs were obtained by varying q_1 from 1.65 to 6 Å and q_2 from 1.45 to 6 Å. A total of 710 ab initio points were interpolated by cubic splines with 0.01 Å resolution to get a grid of 512 × 512 = 262 144 points.

Since we are interested in the dynamics after a vertical excitation, TDM surfaces are only computed in the FC window. Specifically, we have interpolated 16 points between $1.86 < q_1 < 2.05$ Å and $1.68 < q_2 < 1.88$ Å. Outside of this region, the TDM values were set to the value at the closest point of the border of the interpolated region.

2.2. Vibrational Eigenfunctions. The nuclear eigenvalues and eigenfunctions $\varphi^0_{\nu_1\nu_2}(q_1, q_2)$ of the electronic ground state $a^1A'(V_0)$ of CH_2BrCl have been calculated using the Fourier grid Hamiltonian method[22] as implemented in the WavePacket program package.[23] The indices ν_1 and ν_2 indicate nodes along the q_1 and q_2 coordinates, respectively. The molecular Hamiltonian employed in the calculation is the sum of the kinetic energy T and the potential energy $V_0(q_1, q_2)$ (see section 2.1). Using atomic units ($\hbar = 1$), the two-dimensional nuclear kinetic energy operator, $\hat{T}_n$ is given as

$$\hat{T}_n = -\frac{\partial^2}{2m_a\partial^2 q_1} - \frac{\partial^2}{2m_b\partial^2 q_2} - \frac{\cos\theta}{m_c}\frac{\partial^2}{\partial q_1\,\partial q_2} \qquad (1)$$

where θ denotes the Cl−C−Br angle (113.5°), and the reduced masses are computed as,

$$\begin{aligned} m_a &= M_{Br}M_{CH_2}/(M_{Br} + M_{CH_2}) \\ m_b &= M_{Cl}M_{CH_2}/(M_{Cl} + M_{CH_2}) \\ m_c &= M_{CH_2} \end{aligned} \qquad (2)$$

with M_{Br}, M_{Cl}, and M_{CH_2} being the masses of atoms Br, Cl, and that of the radical, CH_2, respectively.

Accordingly, the reduced mass m_a is 11.91 amu, m_b is 10.04 amu, and m_c is 14.00 amu. The calculation was carried out on a regular spatial grid of 64 × 64 points divided evenly between $1.65 < q_1 < 2.28$ Å and $1.45 < q_2 < 2.08$ Å.

2.3. Diabatization of the PES and TDM. The transformation of the adiabatic nuclear wave function, χ^{ad}, to the diabatic one, χ^{di}, is described by the unitary transformation[24]

$$\chi^{di} = \underline{\underline{U}}^{+}\chi^{ad} \qquad (3)$$

In the case of a three-level system with two electronically excited states crossing, the unitary transformation matrix $\underline{\underline{U}}$ has the form

$$\underline{\underline{U}} = \begin{pmatrix} 1 & 0 & 0 \\ 0 & \cos(\tau) & -\sin(\tau) \\ 0 & \sin(\tau) & \cos(\tau) \end{pmatrix} \qquad (4)$$

where the mixing angle τ depends on the internal nuclear coordinates, q_1 and q_2. The diabatic potential matrix, $\underline{\underline{V}}^{di}$, as well as the diabatic transition dipole moment matrix, $\underline{\underline{\mu}}^{di}$, can be computed from the adiabatic ones, $\underline{\underline{V}}^{ad}$ and $\underline{\underline{\mu}}^{ad}$, by the unitary transformations

$$\underline{\underline{V}}^{di} = \underline{\underline{U}}^{+}\underline{\underline{V}}^{ad}\underline{\underline{U}} \qquad \underline{\underline{\mu}}^{di} = \underline{\underline{U}}^{+}\underline{\underline{\mu}}^{ad}\underline{\underline{U}} \qquad (5)$$

In principle, τ can be obtained from ab initio electronic wave functions.[25] This is, however, not possible for the MS-CASPT2

level of theory, and therefore, we approximate $\tau(q_1, q_2)$ by a simple analytical expression whose parameters are fitted as to provide the smoothest diabatic potentials in the crossing window. In the case of a linear near-degenerate crossing line[15] (see later in text), a suitable candidate for $\tau(q_1, q_2)$ is

$$\tau(q_1, q_2) = \frac{\pi}{4} + \frac{1}{2}\arctan(\Gamma D(q_1, q_2)) \tag{6}$$

where $D(q_1, q_2)$ is the distance of any (q_1, q_2) point to the near-degenerate crossing line. Provided this line is defined by

$$q_2 = aq_1 + b \tag{7}$$

$D(q_1, q_2)$ is computed as

$$D(q_1, q_2) = \frac{q_2 - aq_1 - b}{\sqrt{a^2 + 1}} \tag{8}$$

Equations 6 and 8 ensure that the diabatic potentials fit to the adiabatic ones far from the crossing. The width of the coupling region, that is, the decay of the coupling with D, resulting in a smooth V^{di} PES, is controlled by the parameter Γ . Here, Γ is taken as constant, that is, independent of q_1 and q_2. The definition of τ together with a constant Γ is equivalent to approximating the kinetic coupling functions ${}^iT_{12}^{(1)} = \langle\Phi_1|\partial/\partial q_i|\Phi_2\rangle$ in the adiabatic Hamiltonian by Lorentzian functions of D, similar to our previous 1D work.[14] The $|\Phi_k\rangle$ is the electronic wave function of state k in the adiabatic representation. In this case, the equations ${}^iT_{12}^{(1)} = \partial\tau/\partial q_i$ fulfill, and the derivative coupling terms disappear from the Hamiltonian in the diabatic representation (see also refs 26, 27 and 28).

2.4. Quantum Dynamics. The simulation of the photodissociation dynamics is governed by the time-dependent Schrödinger equation (TDSE), which can be written as

$$i\hbar\frac{\partial\chi(q_1, q_2, t)}{\partial t} = \hat{H}(q_1, q_2, t)\chi(q_1, q_2, t) \tag{9}$$

where $\chi(q_1, q_2, t)$ is the nuclear wave function vector, with the elements belonging to the corresponding electronic states, which can be solved in the adiabatic or diabatic representation.[25] In the diabatic representation and in the presence of an external electric field $\underline{E}(t)$, the diabatic Hamiltonian, $\hat{H}^{\mathrm{di}}$ can be written as

$$\hat{H}^{\mathrm{di}}(q_1, q_2, t) = \hat{T}_n + \underline{\underline{V}}^{\mathrm{di}}(q_1, q_2) - \underline{\underline{\mu}}^{\mathrm{di}}(q_1, q_2)\underline{E}t) \tag{10}$$

with the kinetic energy operator $\hat{T}_n$ defined in eq 1. In the diabatic representation, the potential energy matrix, $\underline{\underline{V}}^{\mathrm{di}}(q_1, q_2)$, is nondiagonal, and the off-diagonal elements are the potential coupling elements between the crossing electronic states. Note that in the adiabatic representation, the potential coupling transforms into the nonadiabatic kinetic coupling.[25] If we neglect nonadiabatic kinetic couplings in the adiabatic representation, eq 9 can be solved with the Hamiltonian,

$$\hat{H}^{\mathrm{ad}}(q_1, q_2, t) = \hat{T}_n + \underline{\underline{V}}^{\mathrm{ad}}(q_1, q_2) - \underline{\underline{\mu}}^{\mathrm{ad}}(q_1, q_2)\underline{E}(t) \tag{11}$$

The elements of the transition dipole moment matrix $\underline{\underline{\mu}}^{\mathrm{ad/di}}$ are set to zero, except for $\underline{\mu}_{01}^{\mathrm{ad/di}}$ and $\underline{\mu}_{02}^{\mathrm{ad/di}}$. The diabatic transition dipole moments are calculated according to eq 5 from the ab initio adiabatic ones.

The electric field $\underline{E}(t)$ is modeled in both cases as

$$\underline{E}(t) = \underline{\epsilon}E_0\cos(\omega t)S(t) \tag{12}$$

with polarization vector $\underline{\epsilon}$, amplitude E_0, central frequency ω, and analytical shape function $S(t)$

$$S(t) = \begin{cases} \sin^2(\pi t/t_{\mathrm{p}}) & \text{if } 0 < t < t_{\mathrm{p}} \\ 0 & \text{otherwise} \end{cases} \tag{13}$$

with duration of the pulse t_{p}. To guarantee our results to be comparable with experimental ones obtained with continuous-wave light, the pulse duration must be large enough such that the laser spectral width is small compared with the energy gap between the two excited states in the FC region. For a sine square pulse shape (cf. eq 13), a pulse duration of $t_{\mathrm{p}} = 50$ fs fulfills this condition. This value is used in all the simulations. Note that longer pulses do not change the results qualitatively. The amplitude of the laser field is chosen to be weak enough so that only 10−20% of the population is transferred. The corresponding maximum intensities

$$I_0 = 1/2\epsilon_0 c\underline{E}_0^2 \tag{14}$$

are below the limit of $\sim 10^{13}$ W/cm^2 to avoid ionization or Stark shifts.

Initially, we consider the molecule to be prepared in the vibrational ground state ($\nu_1 = \nu_2 = 0$) of the electronic ground state ($i = 0$), $\varphi^i_{\nu_1\nu_2}(q_1, q_2)$

$$\chi(q_1, q_2, t = 0) = \begin{pmatrix} \varphi^0_{00}(q_1, q_2) \\ 0 \\ 0 \end{pmatrix} \tag{15}$$

Equation 9 has been numerically solved using the Split-Operator scheme[29] and the fast Fourier technique[30] on a grid consisting of 512 × 512 grid points with a time discretization of $\Delta t = 0.01$ fs, as implemented in the WavePacket code.[23] Although we are mainly interested in the dynamics up to 4 Å bond lengths, the wavepacket propagations were performed up to 6 Å where necessary. Artificial back reflection of the wavepacket was avoided by a gobbler function[31] extending over 15 grid points from the borders.

3. Results and Discussion

3.1. Adiabatic PESs and TDMs. The most important PESs to simulate UV photodissociation in the wavelength range of 170−210 nm are those associated to the a^1A', b^1A', and c^1A' states, which we denote as V_0^{ad}, V_1^{ad}, and V_2^{ad}, respectively. Figure 1a−c shows the adiabatic contour plots adapted from ref 15.

The lowest electronically excited state b^1A' (V_1^{ad}) is strongly repulsive along both dissociation channels, C−Br and C−Cl. Upon vertical excitation to the b^1A' state, only C−Br dissociation is expected because the FC window is located on the C−Br slope. In contrast, the adiabatic c^1A' PES shows a well along the line of equidistant C−Br and C−Cl bonds, which could allow for simultaneous fragmentation. As reported in ref 15, the b^1A' and c^1A' states are almost degenerate along this line, forming what we have called a near-degenerate crossing line. Along this line, a CoIn has been identified at q_1 =3.4 Å and q_2 =3.28 Å;[15] see square symbol in Figure 1.

Figure 1 also shows the adiabatic TDM surfaces for the $a^1A' \rightarrow b^1A'$ and $a^1A' \rightarrow c^1A'$ transitions, with x and z components denoted by $\mu_{ij\epsilon}^{\mathrm{ad}}$, where ϵ is either x or z.

3.2. Diabatization, Diabatic PESs, and TDMs. The crossing line of the corresponding diabatic potentials in the q_1 and q_2 2D space is formed by the (q_1, q_2) points for which the energy separation between adiabatic potential energies of the b^1A' and c^1A' states for any fixed q_1 distance is minimal. In the range $1.84 < q_1 < 4.21$ Å and $1.82 < q_2 < 4.07$ Å, this crossing line is found to be almost linear, that is, very close to the $q_1 = q_2$ line. This almost linear shape allows us to approximate the

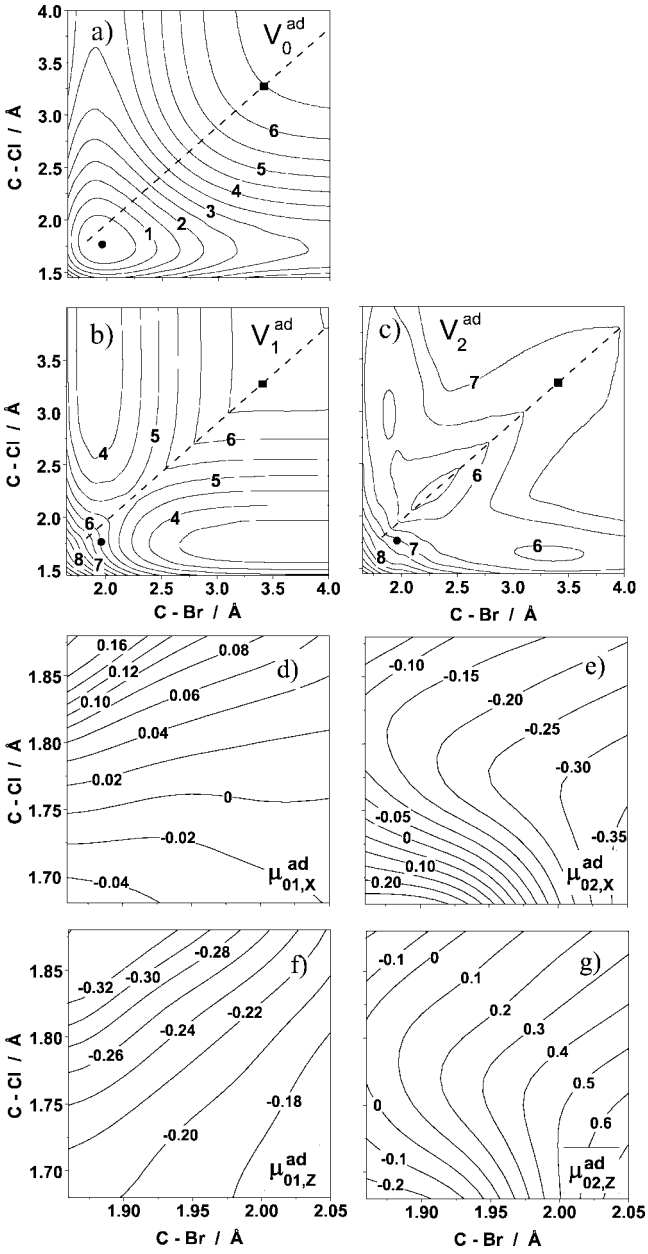

Figure 1. The panels (a−c) show the MS-CASPT2 adiabatic potential energy surfaces V_0^{ad}, V_1^{ad}, and V_2^{ad} adapted from ref 15, with the circle and square symbols indicating the Franck−Condon point and the position of the CoIn, respectively. The contour levels are given in eV. The (d−g) panels display the adiabatic transition dipole moments (TDM), $\mu_{01\epsilon}^{ad}(q_1, q_2)$ and $\mu_{02\epsilon}^{ad}(q_1, q_2)$ near the Franck−Condon region; the values were computed in 16 grid points (4 along C−Br and 4 along C−Cl) within the region indicated in the figures. Outside of this region, the adiabatic TDM values were set to the value at the closest point on the border of the interpolated region. The $\mu_{01\epsilon}^{ad}(q_1, q_2)$ and $\mu_{02\epsilon}^{ad}(q_1, q_2)$ functions were then transformed to the corresponding diabatic TDM functions according to eq 5. Contour levels are given in au.

distance of any point from this line by the analytic expression in eq 8, using $a = 0.94213$ and $b = 0.08084$ Å.

To diabatize the PESs and TDMs surfaces according to eqs 4–6, the Γ parameter is fitted, taking into account two conditions. On the one hand, the diabatic potentials should be smooth so that the diabatic electronic wave functions vary slowly along the avoided crossing. This condition requires a small Γ parameter. On the other hand, the diabatic potentials should converge not too slowly to the adiabatic ones outside of the crossing region; otherwise, one may have a considerable

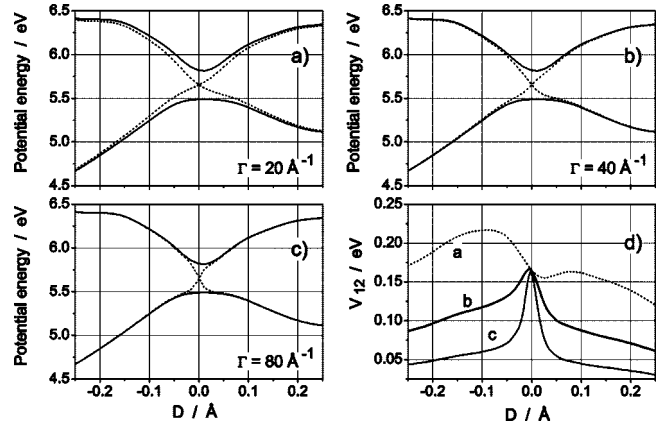

Figure 2. Diabatic potentials (a−c) and corresponding potential coupling (d) for different diabatization parameters Γ. The cut, along which the D is measured, is perpendicular to the near-degenerate crossing line and crosses it at $q_1 = 1.98$ and $q_2 = 2.02$.

TABLE 1: Energies, $E(\nu_1, \nu_2)$, and Transition Energies, $\Delta E(\nu_1, \nu_2) = E(\nu_1, \nu_2) - E(0, 0)$ in cm^{-1} Units, for Selected Ground-State Vibrations Obtained for V_0^{ad}

n	ν_1 ν_2	$E(\nu_1, \nu_2)$	$\Delta E(\nu_1, \nu_2)$
0	00	675	
1	10	1250	575
2	01	1432	757
3	20	1824	1149
4	11	2005	1330
5	02	2181	1506

coupling also far from the crossing, maybe even in regions where one or both adiabatic states already have an electronic structure different from that attributed to the crossing diabatic states. Since in CH_2BrCl the electronic structure of the adiabatic c^1A' state changes very rapidly in the vicinity of the FC region,[15] the latter condition is important.

Figure 2a−c presents the adiabatic and diabatic potentials displayed as a function of the distance D (cf. eq 8) measured perpendicularly from the crossing line in the vicinity of the FC region for Γ values of 20, 40, and 80 Å^{-1}, respectively. Figure 2d shows the potential couplings V_{12} for the three cases. Among them, we find Γ = 40 Å^{-1} to be the most suitable compromise between the above two requirements, that is, fast convergence outside of and smooth behavior within the crossing region. Therefore, in section 3.4, we shall concentrate on the results obtained using Γ =40 Å^{-1}, even if the dependence of the dynamics on the diabatization parameter will be also discussed.

Figure 3 shows the diabatic PESs V_1^{di} and V_2^{di}, as well as the potential coupling V_{12}^{di} computed with Γ = 40 Å^{-1}. V_1^{di} and V_2^{di} no longer change after d(C−Br) > 4 Å and d(C−Cl) > 4 Å, respectively. Thus, once the C−Br (C−Cl) bond length in the diabatic state V_1^{di} (V_2^{di}) reaches the 4 Å limit, the fate of the molecule is sealed; it will irreversibly dissociate along the C−Br (C−Cl) coordinate. Consequently, it is reasonable to focus our dynamical investigations to the d(C−X) < 4 Å range. Figure 3 also shows the diabatized x and z components of the TDM, similar to Figure 1.

3.3. Vibrational Eigenstates. Before discussing the results of the wavepacket dynamics, we shall shortly comment on the obtained vibrational eigenstates of the electronic ground state V_0. The lowest six eigenfunctions are displayed in Figure 4, with the corresponding energies summarized in Table 1. According to the number of nodes, it is straightforward to classify the eigenfunctions as C−Br and C−Cl stretching modes, which are denoted by the quantum numbers ν_1 and ν_2,

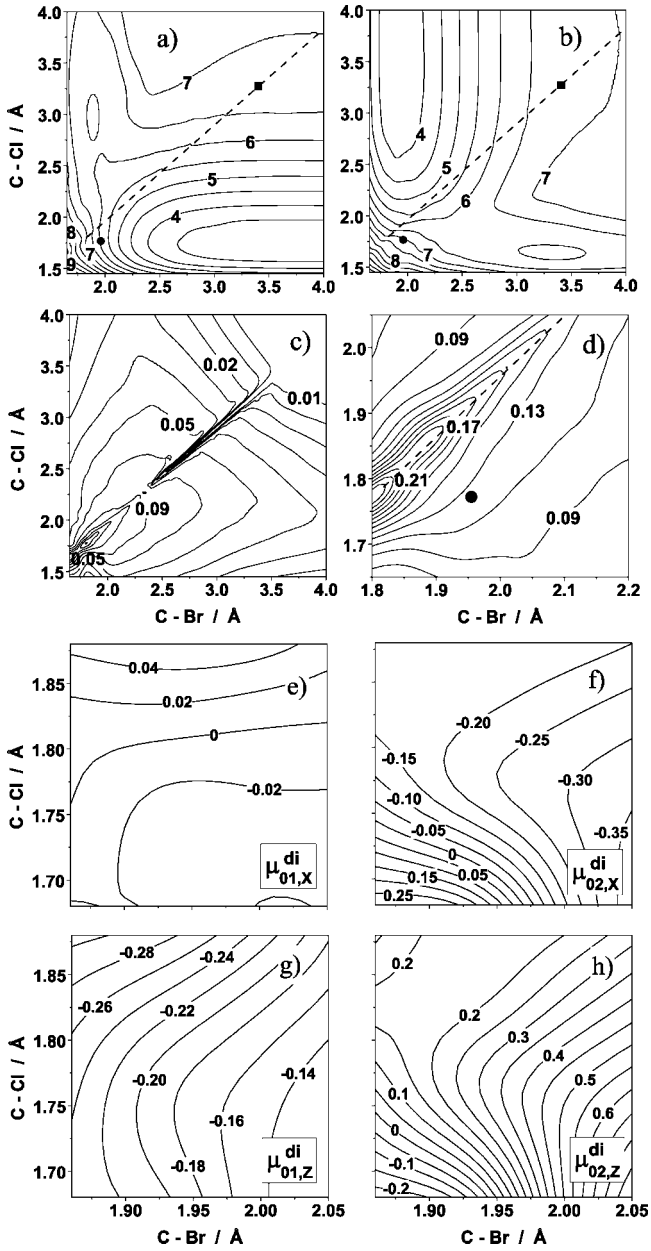

Figure 3. MS-CASPT2 diabatic potential energy surfaces and potential coupling computed with diabatization parameter $\Gamma = 40$ Å^{-1}; (a−c) display potentials V_1^{di} and V_2^{di} and potential coupling V_{12}^{di}, respectively. The black circle and square symbols indicate the Franck−Condon point and the CoIn as in Figure 1. The dashed line shows the pseudodegenerated crossing line; (d) shows V_{12}^{di} in the vicinity of the Franck−Condon region. The contour levels in (c) are scaled logarithmically, and the rest are scaled linearly. Energy values are given in eV. The (e−h) panels display the diabatic transition dipole moments (TDM), $\mu^{di}_{01\epsilon}(q_1, q_2)$ and $\mu^{di}_{02\epsilon}(q_1, q_2)$, near the Franck−Condon region.

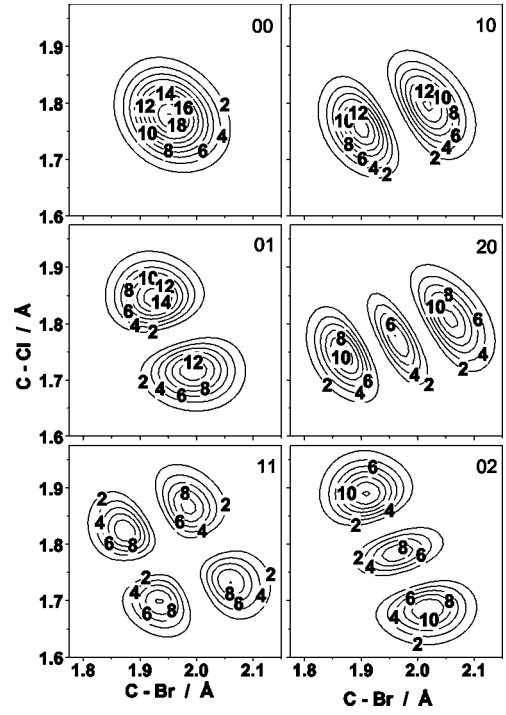

Figure 4. Two-dimensional vibrational eigenfunctions, $|\varphi^0_{\nu_1\nu_2}(q_1, q_2)|$, of CH_2BrCl. The $\nu_1\nu_2$ quantum numbers are displayed in the upper right corner.

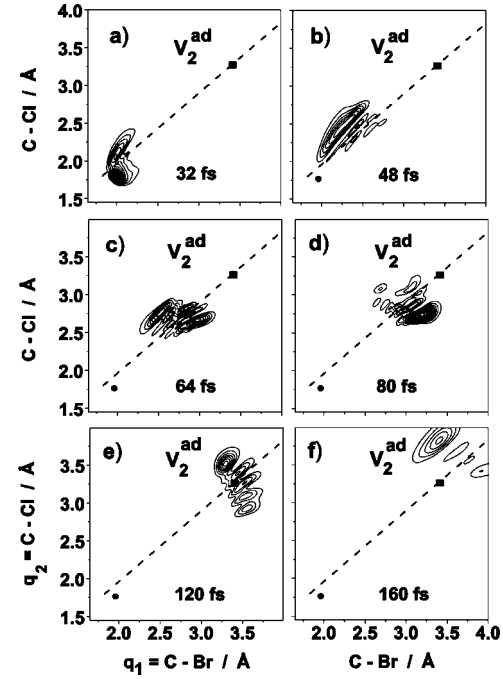

Figure 5. Adiabatic wavepacket propagation on the V_2^{ad} potential upon $\lambda = 177$ nm excitation ($I_0 = 2$ TW/cm^2, $t_p = 50$ fs, $\epsilon = z$).

respectively. As it can be seen from Figure 4, the C−Br and C−Cl vibrations are coupled.

According to the FGH diagonalization method and within our reduced 2D model, the lowest C−Br and C−Cl stretching modes are estimated to be 575 and 757 cm^{-1}. These values are within 6 and 2% off the corresponding experimental values[32] (614 and 744 cm^{-1}). The harmonic vibrational frequencies calculated at the MP2/6-311+G(d,p) level of theory[13] including all degrees of freedom are 617 and 764 cm^{-1}. From these values, as well as from the almost equidistant-calculated spacing (see Table 1), it is clear that both C−X stretching modes are rather harmonic. The differences between the vibrational transition energies given in Table 1 and the corresponding experimental values, especially for the C−Br stretching mode, are due to the reduced dimensionality (2D) of the present model. In particular, it is expected that the coupling between the Br−C−Cl bending and the C−X stretching modes is stronger in the case of C−Br, and our numbers do show this trend.

3.4. 2D Wavepacket Simulations. The dissociation dynamics in the excited electronic states has been studied using laser wavelengths between $\lambda = 206.5$ and 177 nm. These values correspond to resonant adiabatic energy excitations to the b^1A'

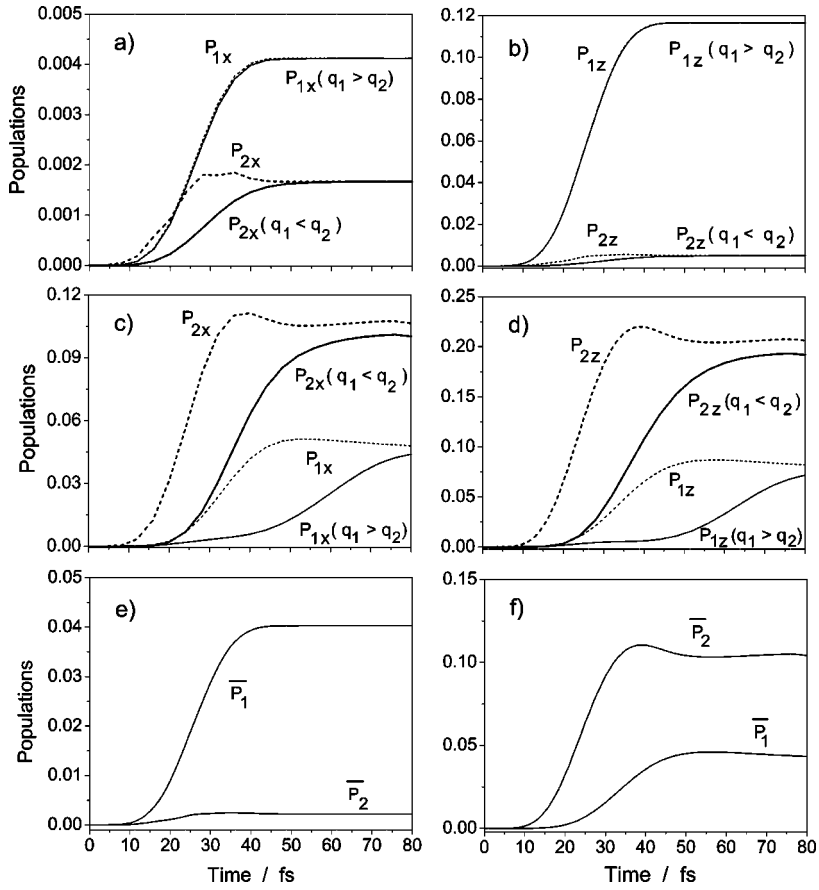

Figure 6. Diabatic population dynamics. Dashed lines in (a) and (b) show the time evolution of populations, $P_{k\epsilon}$, upon excitation by an x- and z-polarized 206.5 nm UV pulse, respectively. Similarly, the dashed lines in (c) and (d) show the time evolution of $P_{k\epsilon}$ upon excitation of an x- and z-polarized 177 nm UV pulse, respectively. The solid lines in (a−d) show the portion of populations on one side of the crossing line. The panels (e) and (f) show the time evolution of the average populations, $\overline{P_k}$ for 206.5 and 177 nm pulses, respectively.

and c^1A' states. In all computations, the electric field amplitude is $E_0 = 3.89$ GV/m, which corresponds to $I_0 = 2.0$ TW/cm^2.

In order to appreciate the effect of the nonadiabatic couplings, we first report the results of wavepacket propagation using adiabatic potentials and transition dipole moments without the coupling between the two excited states. Figure 5 shows the adiabatic wavepacket propagation on electronic state c^1A' induced by the resonant excitation with $\lambda = 177$ nm and laser polarization in the z direction, that is, parallel to the C−Br bond. As it is clear from the snapshots at later times, ignoring the nonadiabatic effects leads to a three-body dissociation, Br + Cl + CH_2 in the potential V_2^{ad}. This simulation should serve as a reference case when the coupling between the b^1A' and c^1A' states is switched on. For this, we solve eq 9 with the Hamiltonian given in eq 10 including the V_0, V_1^{di}, and V_2^{di} diabatic potentials and the coupling V_{12}^{di}. The results are discussed in the following sections.

3.4.1. Time-Dependent Diabatic Population Dynamics. According to the molecular orientation (cf. section 2.1), the TDM of the A′ states have x and z components, and hence, it is possible to photoexcite the preoriented CH_2BrCl with x- or z-linearly polarized light. To consider a uniform distribution of molecular orientations, we perform a classical averaging of the results obtained with each of the three different possible polarization directions of light. Being ϵ the polarization of the electric field (cf. eq 12), then $\mu_{0/\epsilon}^{di}(q_1, q_2)$ is the ϵ component of the TDM between adiabatic states k and l. Furthermore, if $\chi_{k\epsilon}^{di}(q_1, q_2, t)$ denotes the solution of eq 9 under the condition that the electric field is polarized in the ϵ direction, the population of the electronic state k is

$$P_{k\epsilon}(t) = \int_0^\infty \int_0^\infty |\chi_{k\epsilon}^{di}(q_1, q_2, t)|^2 dq_1 dq_2 \qquad (16)$$

The average population $\overline{P_k(t)}$ can be then written as

$$\overline{P_k(t)} = \frac{1}{3}(P_{kx}(t) + P_{kz}(t)) \qquad (17)$$

The population dynamics upon an excitation with the x- and z-polarized field of $\lambda = 206.5$ nm is shown in Figure 6a and b, respectively. Likewise, Figure 6c−d shows the population dynamics upon a 177 nm excitation. Due to the difference magnitude in the TDM (cf. Figure 1), at $\lambda = 206.5$ nm, the population excited with x-polarized field is much smaller than that excited with z-polarized field (note the different scales of Figure 6a and b). At $\lambda = 177$ nm, the x- and z-excited populations are of the same order of magnitude. Also displayed in Figure 6a−d is

$$P_{k\epsilon}(q_1 < q_2) = \int_0^\infty dq_1 \int_{q_1}^\infty dq_2 |\chi_{k\epsilon}^{di}(q_1, q_2, t)|^2 \qquad (18)$$

and the similarly defined $P_{k\epsilon}(q_1 > q_2)$. Their deviation from the corresponding $P_{k\epsilon}$ values tells about the position of the wavepacket with respect to the near-degenerate crossing line. Figures 6e and f present the averaged populations, $\overline{P_k(t)}$ defined by eq 17 for $\lambda = 206.5$ and 177 nm, respectively.

Snapshots of the wave function upon 206.5 and 177 nm excitation are shown in Figures 7 and 8, respectively. Figure 7

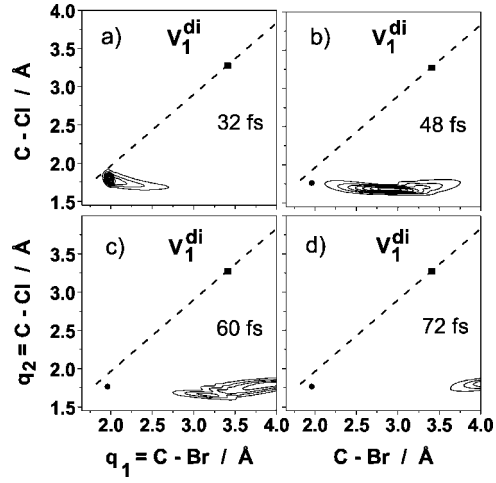

Figure 7. Diabatic wavepacket propagation on the V_1^{di} potential upon $\lambda = 206.5$ nm excitation ($I_0 = 2$ TW/cm^2, $t_p = 50$ fs, $\epsilon = z$). The potential and TDM surfaces were diabatized using $\Gamma = 40$ Å^{-1}. Contour levels are equally spaced, except in (a), where they are two times larger.

collects snapshots only on V_1^{di} since 206.5 nm is resonant with the b^1A' state and the population in V_2^{di} is negligible (see Figure 6e). As expected, upon 206.5 nm excitation, a very fast dissociation into CH_2Cl + Br takes place. Accordingly, $P_1(q_1 > q_2)$ runs parallel to P_1 in Figure 6a and 6b. Also, for $t =$ 72 fs, the center of the wavepacket is already beyond the border d(C−Br) = 4 Å.

The wavepacket dynamics after 177 nm irradiation is more interesting due to the coupling between the excited electronic states. As seen in Figure 8, the wavepacket is vertically created mostly on the $q_1 > q_2$ side of V_2^{di}. Then, it propagates toward larger q_2 (C−Cl) distances, arriving at the $q_2 = 4$ Å border at $t = 76$ fs (50 fs after the peak of the pulse). Note that $P_{2z}(q_1 < q_2)$ (cf. Figure 6d) is close to P_{2z} by this time, implying that all population in V_2^{di} dissociates into CH_2Br + Cl. During this time, the C−Br distance changes to a lesser extent. By the time the UV field is over, the majority of the wavepacket is mostly on the left-hand side of the crossing line but also partially transferred diabatically to the V_1^{di} state. The diabatic χ_1^{di} wave function propagates along the $q_1 = q_2$ line for ∼30 fs until it turns back to the $q_1 > q_2$ side of the PES and dissociates into CH_2Cl + Br before it can reach the CoIn. According to these simulations, three-body dissociation is negligible in the presence of couplings (compare Figure 5 with Figure 8).

Notice in Figure 6d that $P_{1z}(q_1 > q_2)$ is much less than P_{1z} until the wavepacket traverses the near-degenerate line (ca. 50 fs).

In conclusion, we can see that within this model, the wavepacket does not reach the CoIn since it is very efficiently relaxed to the lower state in a few tens of fs. In other words, full nonadiabatic transfer occurs before arriving to the CoIn, as it has been also observed in other nonadiabatic problems; see, for example, ref 33.

3.4.2. Branching Ratio versus Wavelength. Figure 9a shows the total excited populations $\overline{P_1} + \overline{P_2}$ computed at time t_f, at which we assume that the wavepacket propagates irreversibly toward C−Cl on potential V_2^{di} or toward C−Br on potential V_1^{di}. This requirement is fulfilled at $t_f = 80$ fs for 206 nm and within a good approximation for 177 nm. The sum of the averaged excited populations can be considered equivalent to the absorption spectrum, and as such, it shows two broad bands (the Ã and B̃ bands) centered (as expected) around the resonant wavelengths to the V_1^{di} and V_2^{di} states, that is, at 206.5 and 177 nm, respectively.

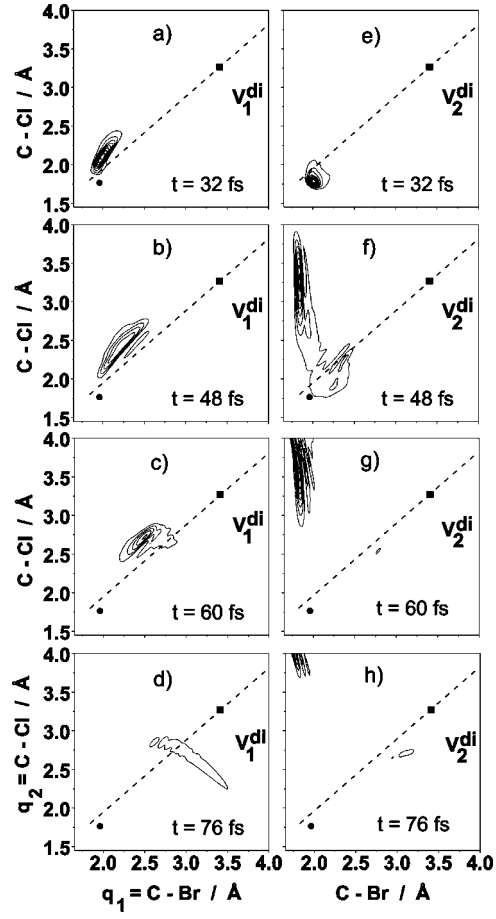

Figure 8. Diabatic wavepacket propagation on V_1^{di} and V_2^{di} potentials upon $\lambda = 177$ nm excitation ($I_0 = 2$ TW/cm^2, $t_p = 50$ fs, $\epsilon = z$). The potential and TDM surfaces are as those in Figure 7. Contour levels are equally spaced, except in (e), where they are four times larger.

From the total populations at t_f, the branching ratio of Br/Cl can be determined as

$$R_\epsilon = P_{1\epsilon}(t_f)/P_{2\epsilon}(t_f) \tag{19}$$

considering a laser linearly polarized along the ϵ direction. The classical average over the different molecular orientations is then

$$\overline{R} = \overline{P_1(t_f)}/\overline{P_2(t_f)} \tag{20}$$

where $\overline{P_1}$ and $\overline{P_2}$ are defined in eq 17. The branching ratios R_x, R_z, and $\overline{R}$ as a function of the wavelength are plotted in Figure 9b. As one can see, at longer wavelengths, the average $\overline{R}$ is closer to R_z since more population is excited with z-polarized light (vide supra). Below 185, nm the Br/Cl ratio is independent of both the laser polarization and the wavelength and is equal to 0.4. This is because in this wavelength region, the majority of the molecules are excited to the c^1A' state and the branching is mainly determined by the nonadiabatic transition to b^1A', regardless of the wavelength. On the contrary, for wavelengths longer than 200 nm, where the majority of the molecules are excited to state b^1A', the branching ratio increases exponentially.

The total excited populations calculated in Figure 9a can be compared with the experimental absorption spectrum.[34,35] Since the first peak in the experimental UV spectrum is located at 202.5 nm[34,35] and our theoretical value is $\lambda^t = 206.5$ nm, we conclude that the theoretical spectrum has a blue shift of $\Delta\lambda^t =$

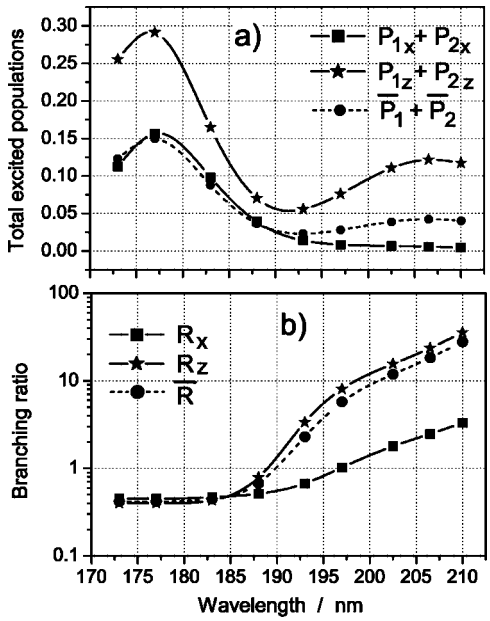

Figure 9. (a) Total excited population as a function of laser wavelength, λ. Asymptotic values of $P_{1\epsilon} + P_{2\epsilon}$ for $\epsilon = x,z$ are represented with the solid lines, and asymptotic values of $\overline{P_1} + \overline{P_2}$ are shown with the dashed line. (b) Branching ratio as a function of λ. R_x and R_z (cf. eq 19) are displayed by solid lines, and the average branching ratio, $\overline{R}$ (cf. eq 20) is displayed by the dashed line.

−4 nm due to an overestimation of the ground-state potential energy with respect to the excited states. This constant shift in energy can be taken into account as a correction in the simulated wavelengths, λ as

$$\lambda' = \lambda - \left(\frac{\lambda}{\lambda^t}\right)^2 \Delta\lambda^t \qquad (21)$$

where λ' is the corrected wavelength, which should be compared with the experiment. With this correction at hand, we go ahead in predicting specific branching ratios to be compared with the scarce experimental values. At $\lambda' = 202.5$ nm, the branching ratio $\overline{R}$ for Br/Cl is predicted to be 23:1. This is in agreement with the observations that almost no C−Cl bond fission occurs at this wavelength.[3] At 193 nm, a branching ratio of 4.5 was measured by Tzeng et al.[5] At $\lambda' = 193$ nm, we predict $\overline{R} = 5.7$, which is in reasonable agreement with the experiment if taking into account the large wavelength dependence of $\overline{R}$ in this wavelength range (see Figure 9b).

At lower wavelengths, no experimental branching ratio is available. The theoretical absorption spectrum predicts a second peak at $\lambda' = 174$ nm, associated with the c^1A' state. Experimentally,[34,35] this state is only present as a shoulder in the UV spectrum. If we deconvolute the measured spectrum in the 164−290 nm range with five Gaussian functions (fewer Gaussians are not enough to resolve the spectrum), the Gaussian belonging to the second excited state is centered at 172.6 nm, in close agreement with our value of 174 nm. At $\lambda' = 174$ nm, our simulations predict a branching ratio of $\overline{R} = 0.4$.

3.4.3. Branching Ratio versus Diabatization Parameter, Γ. Hereafter, we investigate the dependence of the branching ratio upon the diabatization parameter Γ. Branching ratios for Γ = 20, 40, and 80 $Å^{-1}$ and three different wavelengths have been calculated, keeping the rest of the laser parameters fixed. The results are summarized in Table 2. In parentheses, the corresponding shifted λ' are also indicated. As it can be seen, the branching ratio is rather robust at $\lambda' = 202$ or 193 nm. This is due to the fact that when V_1^{di} is excited, the wavepacket dissociates very quickly toward C−Br, and the potential coupling has no effect. Therefore, regardless of the coupling, a majority of C−Br is expected.

At 177 nm, the branching ratio $\overline{R}$ does depend on Γ. The larger that Γ is, the weaker the coupling becomes; recall Figure 2d. Due to the coupling, the wavepacket splits into two parts, one rapidly dissociating toward C−Cl on V_2^{di} and another crossing back and forth the pseudodegenerate crossing line and inducing further nonadiabatic leaking to V_1^{di}, where dissociation along C−Br takes place. Hence, the weaker the coupling is, the lesser population from V_2^{di} that will go nonadiabatically to V_1^{di}, and hence, more C−Cl breakage will be achieved.

For strong couplings, a small portion of the excited-state wavepacket can be trapped in the valley of the adiabatic c^1A' state with enough time to reach the CoIn. If geometry relaxation is considered, concomitant three-body dissociation of a small portion of molecules could also be conceived. On the other hand, the true nature of the CoIn implies that Γ increases toward the CoIn,[36] which acts against being trapped in c^1A' for long times and thus against three-body dissociation.

Noteworthy is also that at 177 nm, the branching ratio is the same for x and z polarization. At longer wavelengths, the R_z is considerably larger than R_x, regardless of Γ.

4. Conclusions

Wavepacket propagations on two-dimensional PESs along the bond distance q_1 (C−Br) and q_2 (C−Cl) have been performed to shed some light onto the nonadiabatic population transfer occurring between the lowest excited states contributing to the $\tilde{A}$ and $\tilde{B}$ absorption bands of CH_2BrCl. These bands can be reasonably well described by the adiabatic b^1A' and c^1A' states, respectively. The former state leads to a strongly repulsive surface dissociative along the C−Br channel, and the latter is strongly coupled with the first along $q_1 = q_2$, showing a conical intersection at C−Br = 3.4 Å and C−Cl = 3.28 Å.

Using a simple diabatization method, three diabatic states are obtained. According to the goals stated in the Introduction, laser-driven propagations using frequencies resonant to the adiabatic b^1A' and c^1A' states show that (i) irradiation to the b^1A' state induces complete dissociation into the $CH_2Cl + Br$ products in less than 100 fs and (ii) irradiation to the c^1A' state leads to

TABLE 2: Branching Ratios, R_ϵ and $\overline{R}$ for Three Different Diabatization Parameters, Γ, at Three Wavelengths λ (Γ in $Å^{-1}$ and wavelength λ in nm)[a]

λ	206.5 (202.5)			197 (193.4)			177 (174)		
Γ	20	40	80	20	40	80	20	40	80
R_z	19	24	33	7.3	8.1	9.2	0.8	0.40	0.15
R_x	2.5	2.5	2.5	1.2	1.0	0.82	0.8	0.45	0.18
$\overline{R}$	15	18	23	5.5	5.7	5.9	0.8	0.42	0.16

[a] In parentheses are the wavelengths, λ', corrected according to eq 21.

$c^1A' \rightarrow b^1A'$ nonadiabatic population transfer after ~30 fs, accompanied by a branching of Br and Cl products. Moreover, the CoIn does not play a key role in the dynamics since nonadiabatic population transfer is complete before the CoIn could be reached. No three-body dissociation occurs within the investigated wavelength range. Finally, we have shown that the Br/Cl branching ratio is strongly influenced by the irradiating wavelength for wavelengths longer than 185 nm. This ratio increases dramatically with wavelengths between 185 and 195 nm and exponentially for higher wavelengths. Below 185 nm, the branching ratio is independent of the wavelength.

The calculated branching ratios are in reasonable agreement with those reported in the literature[5] for different wavelengths, and this agreement improves further upon consideration of a 4 nm blue shift, which is obtained after comparing the experimental and simulated UV absorption spectra. For wavelengths at around 200 nm, we predict 20 times more Br than Cl product, in agreement with the experimental fact that no CH_2Br+Cl dissociation is found.[3,7] According to our simulations, this ratio increases exponentially with wavelengths longer than 200 nm. Additionally, note that the $a^1A' \rightarrow a^1A''$ excitation (not considered here) could also lead to exclusive C−Br bond fission[14] and hence further enhance the Br/Cl ratio at wavelengths longer than 200 nm. At wavelengths shorter than 200 nm, the calculated branching ratios should not depend on the population of b^1A'' since the $a^1A' \rightarrow b^1A''$ transition is much weaker than the $a^1A' \rightarrow c^1A'$.[14] The Br/Cl branching ratio is constant (0.4) for wavelengths below 180 nm. This indicates that it cannot be made smaller by simply selecting a proper wavelength. Moreover, since the minimum branching ratio is the same for both *x*- and *z*-polarized electric fields, tuning the polarization of the field in the molecular frame cannot result in a smaller ratio, either. Decreasing this ratio is thus a proper challenge for quantum control theory.

The Br/Cl branching ratio has been assessed for different Γ diabatization parameters (cf. eq 6). As expected, the wavepacket dynamics changes with the coupling strength only when the adiabatic c^1A' state is populated. A more realistic model requires a coordinate-dependent Γ or a more sophisticated diabatization method,[36] that is, establishing the coupling completely from the shape of the adiabatic potentials. Work along this line is in progress.

Finally, we recall that the role of triplet states have been highlighted in the experiments carried out by Zhou et al.[7] in the 193−266 nm wavelength range, when determining the branching of the final quantum state of product Br atoms. The branching ratios determined herein depend on a singlet−singlet crossing occurring very close to the Franck−Condon region and accessible in a fs time scale.[14,15] Diabatic potential energy matrices including spin−orbit couplings have been recently computed along the two fission coordinates.[37] Therefore, it would be very interesting to investigate whether singlet/triplet crossings, which usually occur on a ps time scale, do influence the here-predicted branching ratios. It should be noted, however, that dynamical effects at longer times inevitably involve IVR, and hence, other degrees of freedom beyond the two fission coordinates need to be taken into account in the dynamics.

Acknowledgment. The Deutsche Forschungsgemeinschaft and the Hungarian Academy of Sciences are acknowledged for financial support (Nr. 436 UNG 113/188/0-1). The authors are grateful to Gy. Lendvay for useful discussions and to H. Köppel for his helpful comments and suggestions for future work.

References and Notes

(1) Wayne, R. P. *The Chemistry of Atmospheres*; Oxford University: New York, 1991.
(2) McGivern, W. S.; Li, R.; Zou, P.; North, S. W. *J. Chem. Phys.* **1999**, *111*, 5771.
(3) Zou, P.; McGivern, W. S.; North, S. W. *Phys. Chem. Chem. Phys.* **2000**, *2*, 3785.
(4) Lee, S.-H.; Jung, Y.-J.; Jung, K.-H. *Chem. Phys.* **2000**, *260*, 143.
(5) Tzeng, W. B.; Lee, Y. R.; Lin, S. M. *Chem. Phys. Lett.* **1994**, *227*, 467.
(6) de Nalda, R.; Izquierdo, J. G.; Irima, D.; Janssen, M. H. M.; Bañares, L. *Femtochemistry VII*; Castleman, A. W., Jr., Kimble, M. L., Eds.; Elsevier: Amsterdam, The Netherlands, 2006; p 49.
(7) Zhou, J.; Kai-Chung, L.; Hassanein, E.; Xu, H.; Tian, S.; Jones, B.; Ng, C. Y. *J. Chem. Phys.* **2006**, *124*, 034309.
(8) Zhang, J.; Heller, E. J.; Huber, D.; Imre, D. G.; Tannor, D. *J. Chem. Phys.* **1988**, *89*, 3602.
(9) Jung, Y.-J.; Park, M. S.; Kim, Y. S.; Jung, K.-H.; Volpp, H.-R. *J. Chem. Phys.* **1999**, *111*, 4005.
(10) Kim, T. K.; Park, M. S.; Lee, K. W.; Jung, K.-H. *J. Chem. Phys.* **2001**, *115*, 10745.
(11) Ji, L.; Tang, Y.; Zhu, R.; Tang, B.; Zhang, B. *Chem. Phys.* **2005**, *314*, 173.
(12) Takayanagi, T.; Yokoyama, A. *Bull. Chem. Soc. Jpn.* **1995**, *68*, 2225.
(13) Rozgonyi, T.; Feurer, T.; González, L. *Chem. Phys. Lett.* **2001**, *350*, 155.
(14) Rozgonyi, T.; González, L. *J. Phys. Chem. A* **2002**, *106*, 11150.
(15) Rozgonyi, T.; González, L. *J. Phys. Chem. A* **2006**, *110*, 10251.
(16) Damrauer, N. H.; Dietl, C.; Kramert, G.; Lee, S.-H.; Jung, K.-H.; Gerber, G. *Eur. Phys. J. D* **2002**, *20*, 71.
(17) Daniel, C.; Full, J.; González, L.; Lupulescu, C.; Manz, J.; Merli, A.; Vajda, S.; Wöste, L. *Science* **2003**, *299*, 536.
(18) Roeterdink, W. G.; Janssen, H. M. H. *Phys. Chem. Chem. Phys.* **2002**, *4*, 601.
(19) Malmqvist, P.-A.; Roos, B. O. *Chem. Phys. Lett.* **1989**, *155*, 189.
(20) Finley, J.; Malmqvist, P.-A.; Roos, B. O.; Serrano-Andrés, L. *Chem. Phys. Lett.* **1998**, *288*, 299.
(21) (a) Andersson, K.; , *MOLCAS 5.0*; University of Lund: Sweden, 2000. (b) Andersson, K.; *MOLCAS 6.0*; University of Lund: Sweden, 2004.
(22) Marston, C.; Balint-Kurti, G. *J. Chem. Phys.* **1989**, *91*, 3571.
(23) Schmidt, B. *WavePacket 4.3: A Program Package for Quantum-Mechanic Wavepacket Propagation and Time-Dependent Spectroscopy*; Free University Berlin: Germany, 2006.
(24) Heumann, B.; Schinke, R. *J. Chem. Phys.* **1994**, *101*, 7488.
(25) Baer, M. *Beyond Born-Oppenheimer: Electronic Nonadiabatic Coupling Terms and Conical Intersections*; Wiley and Sons: Cambridge, U.K., 2006.
(26) Bacchus-Montabonel, M.-C.; Vaeck, N.; Lasorne, B.; Desouter-Lecomte, M. *Chem. Phys. Lett.* **2003**, *374*, 307.
(27) Lasorne, B.; Bacchus-Montabonel, M.-C.; Vaeck, N.; Desouter-Lecomte, M. *J. Chem. Phys.* **2004**, *120*, 1271.
(28) Baer, M. *Chem. Phys. Lett.* **1975**, *35*, 112.
(29) (a) Feit, M. D.; Fleck, J. A.; Steiger, A. *J. Comput. Phys.* **1982**, *47*, 412. (b) Fleck, J. A.; Morris, J. R.; Feit, M. D. *Appl. Phys.* **1976**, *10*, 1929.
(30) Kosloff, D.; Kosloff, R. *J. Comput. Chem.* **1982**, *52*, 35.
(31) Child, M. S. *Mol. Phys.* **1991**, *72*, 89.
(32) Shimanouchi, T. *Tables of Molecular Vibrational Frequencies Consolidated*; National Bureau of Standards: Gaithersburg, MD, 1972; Vol. 1.
(33) Levine, B. G.; Martinez, T. J. *Annu. Rev. Phys. Chem.* **2007**, *58*, 613.
(34) Orkin, V. L.; Khamagonov, V. G.; Guschin, A. G.; Huie, R. E.; Kurylo, M. J. *J. Phys. Chem. A* **1997**, *101*, 174.
(35) Data from www.nist.gov/kinetics/spectra/index.htm.
(36) Köppel, H.; Schubert, B. *Mol. Phys.* **2006**, *104*, 1069.
(37) Valero, R.; Truhlar, D. G. *J. Phys. Chem. A* **2007**, *111*, 8536.

JP8011427